Chapter 11

Thermodynamic analyses of vapour-absorption refrigeration systems

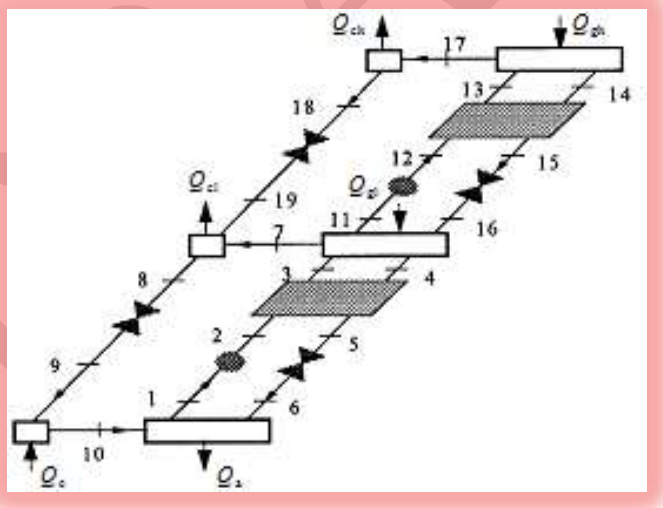

DRAFT

Vapour-absorption refrigeration (VAR) systems do not compress a vapour refrigerant as in the more commonly used vapour-compression refrigeration (VCR) systems. Instead, the refrigerant vapour is dissolved in a liquid absorbent at the lower pressure and the solution is heated to release it at the higher pressure. Thus, VAR systems require considerably less work input than VCR systems. Since a low-temperature heat source can be used for the heating process, VAR systems are important elements for efficient use of energy and for the utilisation of renewable energies such as solar and geothermal energies. Thermax provides two sets of property functions for the two most commonly used absorbent-refrigerant combinations in VAR systems, which are lithium-bromide-water, with water as the refrigerant, and water-ammonia, with ammonia as the refrigerant. This chapter verifies these functions by analysing different types of VAR systems. Initially, the chapter gives a brief review of VAR systems and discusses the temperature-pressure-concentration and enthalpy properties of water-lithium-bromide solutions. It verifies the functions for lithium-bromide-water by comparing the results of analysing a basic VAR system, a single-effect system with a heat-exchanger, and a double-effect system with the data provided by Stoecker and Jones [1], ASHRAE [2], and Abdulateef et. al. [3]. The ammonia-water functions are verified by comparing their results for analysing the single-effect VAR system with those given by Sun [4].

11.1. Vapour-absorption refrigeration systems

Fossil fuels are commonly burnt in industrial, commercial, and residential buildings to produce thermal energy for different uses, but part of the fuels' energy is rejected to the surrounding as waste energy [5]. Large amounts of waste heat are also released to the ambient from the internal combustion engines in the automotive industry and from marine engines [6]. With the increasing world population, the rate at which the non-renewable sources of fossil fuels are being consumed has become a major concern. The increasing costs of fossil fuels and the uncertainties regarding the future prospects of these conventional sources of energy force the scientists and engineers to come up with ideas for making the energy systems more efficient by developing appropriate technologies to recover and utilise the waste heat [7]. Recovering the waste heat from the utility power plants that burn fossil fuels also helps to reduce the CO_2 emissions which is responsible for the global environmental problem of greenhouse effect [5]. One of the technologies that is suitable in terms of energy efficiency and economic feasibility is to utilise the waste heat for the implementation of vapour absorption refrigeration systems for air-conditioning and cooling purposes.

In both VAR systems and VCR system the cooling effect is achieved by the vaporisation of a refrigerant in an evaporator, but the operating principle of VAR systems has two major differences from that of VCR systems [8]. Firstly, unlike the VCR system, a secondary fluid is used in the system as an absorbent for the refrigerant. Secondly, while a VCR system requires mechanical energy to drive it, the VAR system requires heat energy to drive it. Figure 11.1 shows a line diagram of the basic VAR system. A weak solution at state 1 is pumped from the absorber to the generator that desorbs the refrigerant from the absorbent at the high pressure. A heat source provides heat to the

DRAFT

generator to vaporise the refrigerant. Once the refrigerant vaporises, it is led at state 3 to the condenser where it dissipates heat to the environment while changing its phase from vapour to liquid state at state 4. The liquid refrigerant is then throttled to reduce its pressure before taken to the evaporator to absorb heat from the cooling space to vaporise and then returned to the absorber. The strong solution left in the generator is also throttled to the low pressure and returned to the absorber. Figure 11.2 shows a schematic drawing of a commercial VAR unit that implements the basic cycle that has two pressure levels.

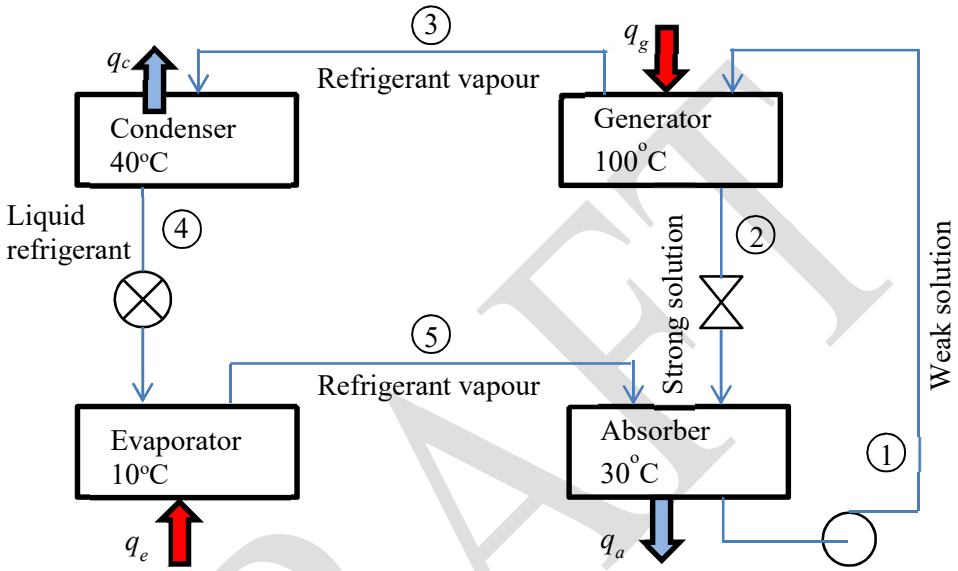

Figure 11.1. Simple VAR system (adapted from Stoecker and Jones [1])

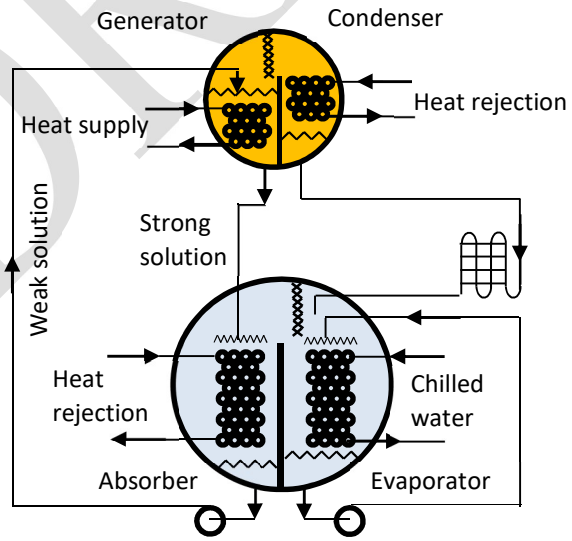

Figure 11.2. Schematic of a commercial VAR unit (adapted from [9])

DRAFT

Since the generator and condenser operate at the high pressure level, while the evaporator and absorber operate at the low pressure level, the generator and condenser are contained in one vessel and the evaporator and absorber are contained in another. The two solutions most commonly used in commercial VAR systems are ammonia-water (ammonia is refrigerant) and water-lithium bromide (LiBr) (water is refrigerant). Lithium bromide is a solid salt crystal which, in the presence of water vapour, will absorb the vapour and become a liquid solution. Although the working principle of the VAR systems using the two solutions is the same, there are some crucial differences between them regarding the volatility of the absorbent, the difference in pressure levels, and the solubility ranges [8]. Since ammonia has a lower latent heat of vaporisation compared to water, the mass-circulation rates of NH_3-H_2O systems are roughly double those of H_2O-LiBr systems for the same duty.

Due to the small boiling point difference between ammonia and water, both ammonia and water boil out from the solution in the generator of a NH_3-H_2O system. Therefore, this system needs a rectification column, a dephlegmator, and a sub-cooling heat exchanger in addition to the main components shown on Figure 11.1. While H_2O-LiBr systems operate under vacuum pressure, NH_3-H_2O systems work at a pressure much higher than the atmospheric pressure. The high affinity of the H_2O-LiBr pair, low volatility, low corrosive action, low-pressure operation, and eliminating the need for a rectifier makes it preferred over the ammonia-water mixture [8]. Therefore, it is substantially used in medium and large-capacity air conditioning and refrigeration systems. However, because of water this system cannot be used under sub-zero temperature conditions [8]. Since the freezing point of ammonia is -77°C, the ammonia-water VAR system is preferred for refrigeration processes requiring low temperatures (less than -5^0C). Unlike water, ammonia is both toxic and flammable.

The coefficient of performance (COP) of a VAR system depends on the heat-source temperature and, to some extent, the cooling-water temperature. Although the COP of the VAR system varies from 0.65 to 0.75, which is significantly lower than that of a comparable VCR system, its important advantage is that the required supply of heat can come from a low-grade heat source, such as the exhaust gas of an engine, or a renewable source of energy such as solar energy, geothermal energy, or biomass. One of the limitations of the simple VAR system shown on Figure 11.1 is that it cannot take advantage of the availability of high temperature heat sources to achieve a higher COP. Even with the use of heat-exchangers between its hot and cold stream, the COP of a single-effect lithium-bromide-water machine is essentially independent of the heat input temperature and remains around 0.7 [10]. When a high-temperature source is available, a double-effect VAR system can be used. The major distinguishing feature of this system is that it incorporates a second generator which uses the condensing water vapour from the first generator to get its supply of heat (Refer to Section 11.5). More detailed information about VAR systems can be obtained from [1], [2], [9], [10], [11], and [12].

DRAFT

11.2. Temperature-pressure-concentration of LiBr-water solutions

As Figure 11.2 shows, both the absorber and generator contain a solution of Li-Br and water above which there is water vapour, while the condenser and evaporator contain pure water in the liquid and vapour phases. Due to simultaneous existence of liquid and vapour of pure water, saturated conditions prevail in the condenser and evaporator. At equilibrium, the pressures in the evaporator and condenser are equal to those of pure water at the corresponding saturation temperatures. Being in the same vessels, the pressures prevailing in the absorber and generator are the same as those of the evaporator and condenser, respectively. Therefore, the condensing temperatures in the evaporator and condenser fix the two pressure levels in the system. However, the temperatures in the absorber and generator depend on both the solution's pressure and concentration in the component. For each combination of pressure and temperature, equilibrium in the LiBr-water solution occurs at a certain concentration as shown by the temperature-pressure-concentration diagram in Figure 11.3. The abscissa of the graph is the temperature of the LiBr solution and the ordinate is the water-vapour pressure shown on the vertical scale on the right. The saturation temperature of pure water corresponding to these vapour-pressures is shown as the ordinate on the left. The chart applies to saturated conditions where the solution is in equilibrium with water vapour.

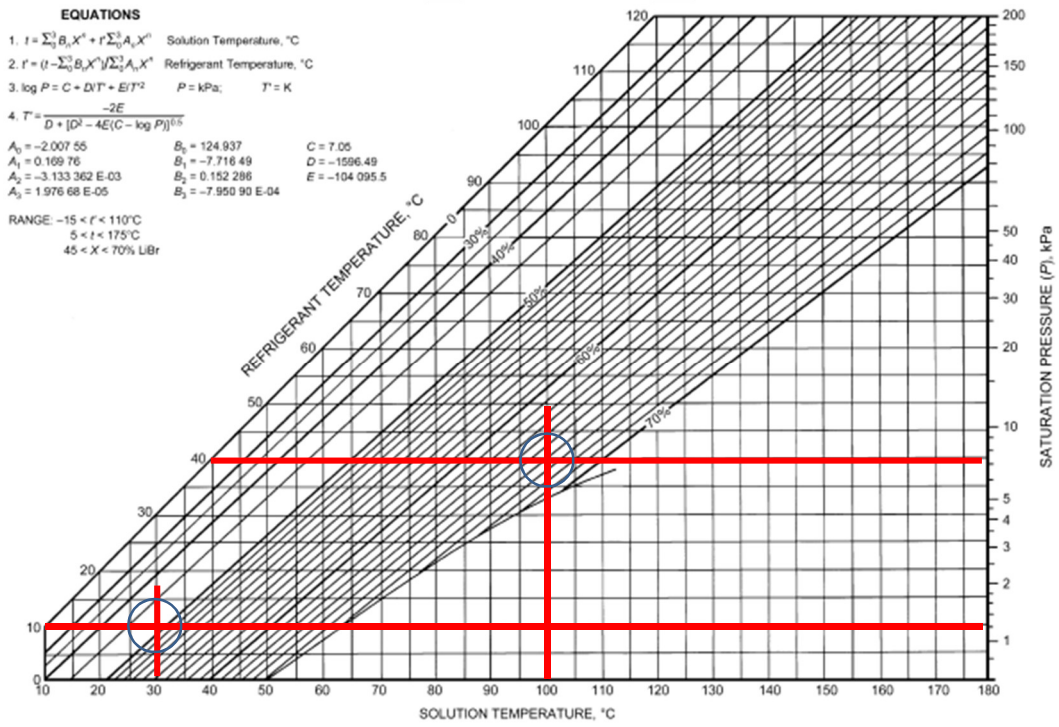

Figure 11.3. Temperature-pressure-concentration diagram of saturated LiBr-water solutions (adopted from ASHRAE [2])

The computation of the mass flow rate in the VAR system incorporates material balances using applicable concentrations of the LiBr in the solution that can be evaluated from the chart in Figure 11.3. For illustration, consider the basic cycle shown on Figure 11.1. Since the temperature in the evaporator is 10°C, the pressure exerted by the vapour is 1.23 kPa as shown on the right vertical scale in Figure 11.3 and the concentration of the LiBr-water solution in the absorber, which is at a temperature of 30°C, is approximately 50%. Similarly, the solution's concentration in the generator can be determined based on the vapour pressure of water at the condenser's temperature of 40°C and the temperature of the generator, which is 100°C. From Figure 11.3, the solution's concentration is about 66%. The following example that illustrates the use these concentrations for determining the mass flow rates in the cycle is based on Example 17-2 in Stoecker and Jones [1].

Example 11.1.
The pump of the cycle shown in Figure 11.1 delivers 0.6 kg/s when the following temperatures prevail: generator, 100°C, condenser, 40°C, evaporator, 10°C; and absorber, 30°C. Compute the flow rate of refrigerant (water) through the condenser and evaporator.

Solution
The following two mass-flow balances can be written about the generator:

Total mass-flow balance:

$$\dot{m}_1 = \dot{m}_2 + \dot{m}_3 \tag{11.1}$$

LiBr balance:

$$\dot{m}_1 X_1 = \dot{m}_2 X_2 \tag{11.2}$$

The values determined above by using the graph of Figure 11.3 for X_1 and X_2 are 50% and 66%, respectively. Substituting the values of $\dot{m}_1$, X_1, and X_2 in Equation (11.2) gives:

$$(0.6)(0.50) = \dot{m}_2 (0.66) \tag{11.3}$$

Which gives $\dot{m}_2 = 0.455$ kg/s. Substituting for $\dot{m}_1$ and $\dot{m}_2$ in Equation (11.1) gives $\dot{m}_3 = 0.145$ kg/s. Approximately 4 kg of solution is pumped for each kilogramme of refrigerant water vapour generated.

11.3. Enthalpy of a LiBr-water solution

In order to determine the heat-transfer rates and COP of the absorption refrigeration cycle, enthalpy data must be available for the working substances at all state points in the cycle. Since pure water in liquid or vapour forms flows in and out of the condenser and evaporator, enthalpies at points 4 and 5 can be determined by using property tables, charts, or functions for water. For the LiBr-water solutions in the generator and absorber,

DRAFT

the enthalpy is a function of the solution's concentration and temperature or pressure. Enthalpies at the exit points of these two components can be determined by using property tables, charts, or functions for the LiBr-water solution [2]. The following example illustrates the use of Thermax functions for determining the enthalpies of water and LiBr-water solution. The example is based on Example 17-3 in Stoecker and Jones [1] who used a chart to determine the enthalpy of the LiBr-water solution.

Example 11.2.
For the absorption system shown in Figure 11.1, compute: Q_G, Q_A, Q_C, Q_E, and the COP of the system at the same temperatures shown on the figure.

Solution
Using the notation of Figure 11.1, the rates of heat transfer at each of the four components are determined by the following energy balances:

Generator:

$$Q_G = \dot{m}_3 h_3 + \dot{m}_2 h_2 - \dot{m}_1 h_1 \tag{11.4}$$

Condenser:

$$Q_C = \dot{m}_3 h_3 - \dot{m}_4 h_4 \tag{11.5}$$

Absorber:

$$Q_A = \dot{m}_2 h_2 + \dot{m}_5 h_5 - \dot{m}_1 h_1 \tag{11.6}$$

Evaporator:

$$Q_E = \dot{m}_5 h_5 - \dot{m}_4 h_4 \tag{11.7}$$

Ignoring the pumps work, the cycle's COP is calculated from:

$$COP = Q_E / Q_G \tag{11.8}$$

Figure 11.4 shows the Excel sheet developed for applying the above analytical model and Figure 11.5 reveals the formulae used in it. On the left side of the sheet are the four temperatures at the evaporator, absorber, condenser, and generator, and the mass flow rate of the solution delivered by the pump. Based on the specified temperatures, the sheet determines the two pressure levels in the system, P_e and P_c, in cells E2 and E3, respectively, using Thermax function from the water group, WatPsat_T. The absorber pressure, P_a, is then made equal to the evaporator's pressure and the generator pressure, P_g, equal to the condenser's pressure in cells E5 and E6, respectively.

DRAFT

COP =Q_e/Q_g

	A	B	C	D	E	F	G	H	I	J	K	L	M	N	O
1															
2	T_e	10	oC	P_e	1.23	kPa	X_1	49.14235		h_1	58.93256		Q_g	13.70055	kW
3	T_a	30	oC	P_c	7.38	kPa	X_2	66.16983							
4	T_c	40	oC							h_2	259.1477		Q_c	10.75656	kW
5	T_g	100	oC	P_a	1.23	kPa	m_2	0.012378							
6				P_g	7.38	kPa				h_3	2675.57		Q_a	13.02995	kW
7	m_1	0.016667	kg/s				m_3	0.004289							
8										h_4	167.53		Q_e	10.08596	kW
9							m_4	0.004289							
10										h_5	2519.21		COP	0.736172	
11							m_5	0.004289							
12															

Figure 11.4. Excel sheet for Example 11.2 using Thermax functions

N14

	A	B	C	D	E	F	G	H
1								
2	T_e	10	oC	P_e	=WatPsat_T(T_e)	kPa	X_1	=LibX_TPr(T_a,P_a)
3	T_a	30	oC	P_c	=WatPsat_T(T_c)	kPa	X_2	=LibX_TPr(T_g,P_g)
4	T_c	40	oC					
5	T_g	100	oC	P_a	=P_e	kPa	m_2	=m_1*X_1/X_2
6				P_g	=P_c	kPa		
7	m_1	=1/60	kg/s				m_3	=m_1-m_2
8								
9							m_4	=m_3
10								
11							m_5	=m_3
12								

(a)

	I	J	K	L	M	N	
		h_1	=LiBh_TX(T_a,X_1)		Q_g	=m_3*h_3+m_2*h_2-m_1*h_1	kW
		h_2	=LiBh_TX(T_g,X_2)		Q_c	=m_3*h_3-m_4*h_4	kW
		h_3	=Wath_Tx(T_g,1)		Q_a	=m_2*h_2+m_5*h_5-m_1*h_1	kW
		h_4	=Wath_Tx(T_c,0)		Q_e	=m_5*h_5-m_4*h_4	kW
		h_5	=Wath_Tx(T_e,1)		COP	=Q_e/Q_g	

(b)

Figure 11.5. The formulae and Thermax functions used in the Excel sheet

Using the pressures thus determined with the specified temperatures at the absorber and generator, the sheet calculates the solution concentrations X_1 and X_2, in cells H2 and H3, respectively, by using Thermax function **LiBX_TPr**. Consequently, the various mass flow rates $\dot{m}_2$ to $\dot{m}_5$ are calculated in cells H5 to H11. The five enthalpy values h_1 to h_5 are then determined by using Thermax function **LiBh_TX** for h_1 and h_2 and **Wath_TX** for h_3, h_4, and h_5. Finally, the sheet calculates the rates of heat transfer at the four components and the cycle's COP based on Equations (11.4) to (11.8). Table 11.1 compares the solution concentrations and rates of heat transfer determined by the present

Excel sheet with their corresponding values given by Ref. [1] who used property tables and charts to determine the various properties. Although the deviations in the heat-transfer rates amount to 4%, the COP is accurately estimated by the present Excel sheet.

Table 11.1. Comparison of the present results with those given by Ref. [1]

	Ref. [1]	Present model	Deviation (%)
X_1	50.0	49.142	-1.715
X_2	66.4	66.170	-0.347
Q_G	473.3	493.220	4.209
Q_C	371.2	387.236	4.320
Q_A	450.3	469.078	4.170
Q_E	348.2	363.095	4.278
COP	0.736	0.7362	0.023

11.4. Analysis of the single-effect system with a heat-exchange

Figure 11.6 shows a Dühring (*P-T*) diagram of a single-effect VAR system that adds a heat-exchanger to the basic system between the strong and weak LiBr-water solutions. By utilising part of the thermal energy in the strong solution for preheating the weak solution before reaching the generator, it minimises the required external heat-input and improves the system's COP.

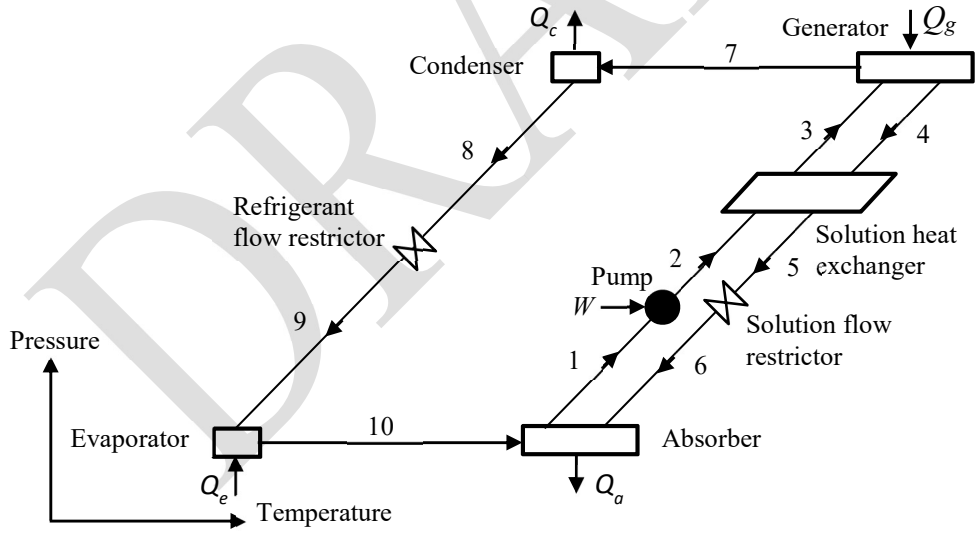

Figure 11.6. The single-effect VAR system with a solution heat-exchanger

11.4.1. The analytical model

The analytical model is based on the following assumptions [2]:

- All system components are at steady-state conditions.
- The kinetic and potential energy of all streams of the VAR system are negligible.

DRAFT

- The refrigerant leaving the condenser is saturated liquid at the condenser pressure and that leaving the evaporator is saturated vapour at the evaporator pressure.
- The condenser pressure is equal to the generator pressure and the evaporator pressure is equal to the absorber pressure.
- There is no pressure drop in the heat exchangers or piping systems.
- There are no heat losses or gains in the various components and piping systems.

Determination of the temperatures and concentrations:

$$T_2 = T_a \tag{11.9}$$

$$T_4 = T_g \tag{11.10}$$

$$T_5 = T_4 - \varepsilon(T_4 - T_2) \tag{11.11}$$

Where ε is the effectiveness of the solution heat-exchanger. The temperatures T_3 and T_6 are determined based on the solution's enthalpy, h_3 or h_6, and concentration X_3 or X_6.

The solution concentrations X_1 and X_4 are determined based on the given temperatures T_a and T_g and the calculated pressures P_a and P_g. For other states:

$$X_3 = X_2 = X_1 \tag{11.12}$$

$$X_6 = X_5 = X_4 \tag{11.13}$$

Calculation of mass flow rates:

$$\dot{m}_3 = \dot{m}_2 = \dot{m}_1 \tag{11.14}$$

$$\dot{m}_4 = \dot{m}_3 X_3 / X_4 \tag{11.15}$$

$$\dot{m}_6 = \dot{m}_5 = \dot{m}_4 \tag{11.16}$$

$$\dot{m}_7 = \dot{m}_3 - \dot{m}_4 \tag{11.17}$$

$$\dot{m}_{10} = \dot{m}_9 = \dot{m}_8 = \dot{m}_7 \tag{11.18}$$

Determination of enthalpies
The enthalpies h_1, h_4, and h_5 are determined at the given temperatures and concentrations using Thermax property function **LiBh_TX** and the enthalpies h_7, h_8, h_{10} at the given or calculated temperatures are determined form the properties of water. Enthalpy values at the remaining four states are obtained as follows:

$$h_2 = h_1 \tag{11.19}$$

DRAFT

$$h_3 = h_2 + \frac{\dot{m}_4}{\dot{m}_2}\left(h_4 - h_5\right) \tag{11.20}$$

$$h_6 = h_5 \tag{11.21}$$

$$h_9 = h_8 \tag{11.22}$$

Determination of heat-transfer rates and COP:
In terms of flow rates and fluid enthalpies, the heat rejected in the absorber Q_a, the heat absorbed in the evaporator Q_e, the heat provided to the generator (desorber) Q_g, the heat rejected in the condenser Q_c and the pump work w_p are given by:

$$Q_e = \dot{m}_9\left(h_{10} - h_9\right) \tag{11.23}$$

$$Q_a = \dot{m}_1 h_1 - \dot{m}_6 h_6 - \dot{m}_{10} h_{10} \tag{11.24}$$

$$Q_g = \dot{m}_3 h_3 - \dot{m}_4 h_4 - \dot{m}_7 h_7 \tag{11.25}$$

$$Q_e = \dot{m}_7\left(h_7 - h_8\right) \tag{11.26}$$

$$W_p = \dot{m}_1\left(h_2 - h_1\right) = \dot{m}_1 v_1\left(P_2 - P_1\right) \tag{11.27}$$

The coefficient of performance of the VAR system is defined as:

$$COP = Q_e / \left(Q_g + W_p\right) \tag{11.28}$$

11.4.2. Illustrative examples

Two examples are given in this section to illustrate the use of Thermax functions for energy analyses of this system with different capacities and operating conditions. While the first system is a medium-size absorption chiller operating at relatively low evaporator temperature and high generator temperature [2], the second system is a 3 kW solar-driven refrigeration system operating at various generator temperatures [3].

Example 11.3. Analysis of a medium-size absorption chiller

An absorption chiller that has a cooling capacity, Q_{evap}, of 2148 kW operates with a lithium-bromide-water solution according to the single-effect cycle shown on Figure 11.6. Determine the rates of heat transfer and COP of the chiller with the following data.

T_{evap} = 1.8°C,
T_{cond} = 46.2°C,
T_{abs} = 40.7°C,
T_{gen} = 103.5°C,
Heat-exchanger effectiveness (ε) = 0.654

DRAFT

Mass flow rate of the weak solution, m_1 = 12 kg/s
Refrigerant vapour leaving generator is at equilibrium temperature of the weak solution at the generator pressure
Pump is isentropic.

The Excel model

Figure 11.7 shows the Excel sheet developed for this example. The left side of the sheet shows the given data while the calculations part in the middle of the sheet determines the evaporator and condenser pressures as those given by the saturation pressures of water at the given temperatures and determines the values of concentrations, mass flow rates, temperatures, and enthalpies at the different points in the cycle. The results part on the right side of the sheet determines the various rates of heat and work transfer in the cycle before calculating the COP. Figure 11.8 reveals the formulae used in the sheet with Themax property functions for the lithium bromide-water solution. Table 11.2 that compares the pressures, temperatures, concentrations, the various heat-transfer rates and the COP obtained by the sheet with the corresponding values given by ASHRAE [2] shows minor differences between the results of the two models.

N8 =Q_e/(Q_g+Wp)

	A	B	C	D	E	F	G	H	I	J	K	L	M	N	O
1															
2	Q_evap	2148	kW	P_e	0.703		x_1	60.081		h_1	117.490		Q_g	3124.09	
3	T_e	1.8	oC	P_c	10.252		x_3	60.081		h_2	117.490		Q_c	2306.45	
4	T_c	46.2	oC	P_a	0.703		x_4	64.559		h_3	186.3772		Q_a	2965.64	
5	T_a	40.7	oC	P_g	10.252					h_4	257.383		Q_e	2148.00	
6	T_g	103.5	oC	T_2	40.7		m_2	12.000		h_5	183.362		Q_HEX	826.64	
7				T_3	76.45		m_3	12.000		h_6	183.362		Wp	0.067195	
8	ε	0.654		T_4	103.5		m_4	11.167560		h_7	2674.650		COP	0.688	
9				T_5	62.43		m_5	11.167560		h_8	193.448				
10	m_1	12	kg/s	T_6	49.72		m_6	11.167560		h_9	193.448				
11				T_7	92.59		m_7	0.929568		h_10	2504.199				
12				T_8	46.2		m_8	0.929568							
13				T_9	1.8		m_9	0.929568							
14				T_10	1.8		m_10	0.929568							
15															

Figure 11.7. The Excel sheet developed for analysing the system in Example 11.3

N19

	A	B	C	D	E	F	G	H	I	J	K	L	M	N
1														
2	Q_evap	2148	kW	P_e	=WatPsat_T(T_e)		x_1	=LibX_TTr(T_a,T_e)		h_1	=LiBh_Tx(T_a,x_1)		Q_g	=m_4*h_4+m_7*h_7-m_3*h_3
3	T_e	1.8	oC	P_c	=WatPsat_T(T_c)		x_3	=x_1		h_2	=h_1		Q_c	=m_7*(h_7-h_8)
4	T_c	46.2	oC	P_a	=P_e		x_4	=LibX_TTr(T_g,T_c)		h_3	=h_2+m_4*(h_4-h_5)/m_2		Q_a	=m_5*h_5+m_10*h_10-m_2*h_2
5	T_a	40.7	oC	P_g	=P_c					h_4	=LiBh_Tx(T_g,x_4)		Q_e	=m_10*(h_10-h_8)
6	T_g	103.5	oC	T_2	=T_a		m_2	=m_1		h_5	=LiBh_Tx(T_5,x_4)		Q_HEX	=m_2*(h_3-h_2)
7				T_3	=LiBt_hx(h_3,x_3)		m_3	=m_1		h_6	=h_5		Wp	=m_1*LiBv_Tx(T_a,x_1)*(P_c-P_e)
8	ε	0.654		T_4	=T_g		m_4	=(m_3)*x_3/x_4		h_7	=Wath_PT(P_c,T_7)		COP	=Q_e/(Q_g+Wp)
9				T_5	=T_4-ε*(T_4-T_2)		m_5	=m_4		h_8	=Wath_Tx(T_c,0)			
10	m_1	12	kg/s	T_6	=LiBt_hx(h_6,x_4)		m_6	=m_5		h_9	=h_8			
11				T_7	=T_g		m_7	=m_10		h_10	=Wath_Tx(T_e,1)			
12				T_8	=T_c		m_8	=m_10						
13				T_9	=T_e		m_9	=m_10						
14				T_10	=T_e		m_10	=Q_evap/(h_10-h_9)						
15														

Figure 11.8. The formulae in the Excel sheet of Figure 11.7 for the system in Example 11.3

Table 11.2. The results obtained by the present model compared to those of Ref. [2]

	Ref. [2]	Present		Ref. [2]	Present
P_{evap}	0.697	0.703	$\dot{m}_{evap}$	0.93	0.93
P_{cond}	10.2	10.252	$\dot{m}_6$	11.06	11.168
T_3	76.1	76.45	Q_{evap}	2148	2148.00
T_5	62.4	62.43	Q_{cond}	2322	2306.45
T_6	49.9	49.72	Q_{abs}	2984	2965.64
T_7	92.4	92.59	Q_{gen}	3158	3124.09
T_8	46.2	46.2	Q_{sol}	825	826.64
X_1	59.6	60.081	COP	0.68	0.688
X_6	64.6	64.559			

The performance of this improved system can be compared to that of basic system without the heat-exchanger by setting the heat-exchanger's effectiveness to zero and Figure 11.9 shows the Excel sheet with this adjustment. Note that $T_3 = T_2$ and $T_5 = T_4$. The figure shows that the COP has dropped to 0.544. This means that the heat-exchanger has improved the system's COP by more than 26%. To improve the COP further, a second heat-exchanger can be placed between the cold water exiting the condenser and the hot vapour exiting the evaporator. Proving this is left as an exercise (Problem 11.3).

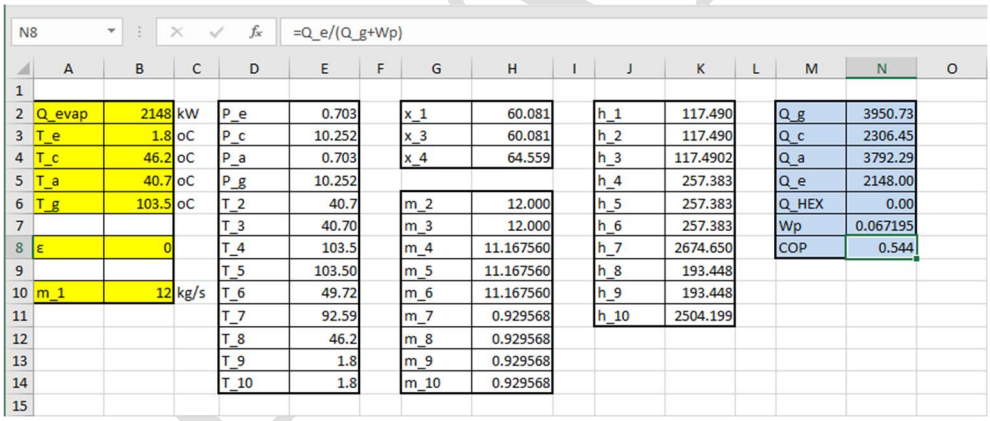

Figure 11.9. Performance of the basic system under the same operating conditions

Example 11.4. Analysis of a solar-driven absorption refrigerator

A solar-driven absorption refrigerator with the single-effect configuration shown on Figure 11.6 uses water-lithium bromide as the working fluid. Analyse the performance of the refrigerator for generator temperatures of 70 to 90°C with the following data [3]:

$T_e = 5$°C,
$T_c = T_a = 35$°C,
Mass flow rate of the weak solution. $m_1 = 0.016$ kg/s,
Heat-exchanger effectiveness (ε) = 0.7,

Mechanical efficiency of the pump (η_p) = 0.8.

The Excel model

Development of the Excel sheet for this example requires minor modifications to that developed for Example 11.3 and Figure 11.10 shows the modified Excel sheet. The particular case shown on Figure 11.10 is the case where T_g = 80°C. Table 11.3 compares the temperatures, concentrations, and enthalpy values at the different states in the cycle as obtained by the present model with their respective values given by Abdulateef et. al. [3]. The figures on the table show that Thermax functions give accurate estimations of the three fluid properties.

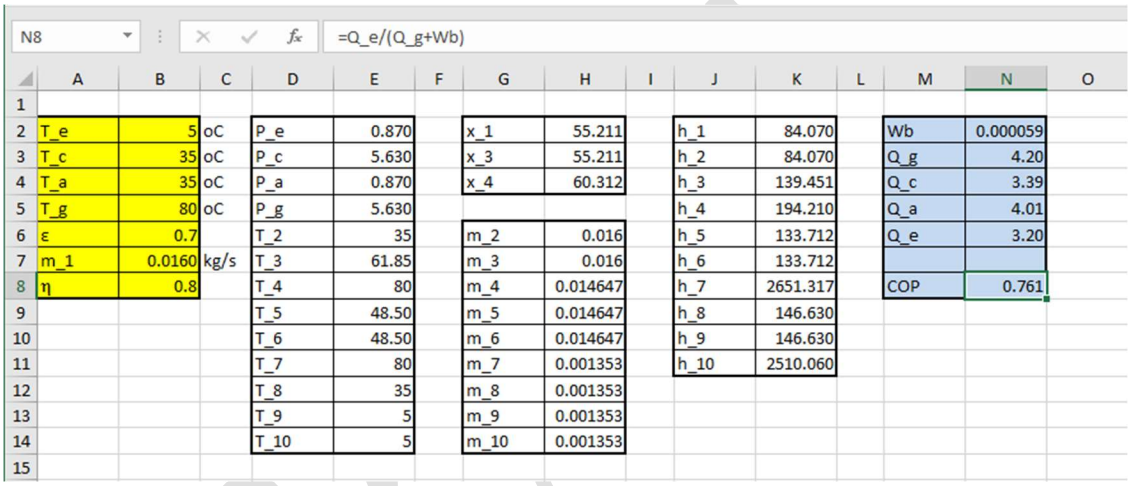

Figure 11.10. The Excel sheet developed for the water-lithium bromide VAR cycle

Table 11.3. Comparison of the temperatures, concentrations, and enthalpies calculated by the present model with those of Ref. [3]

	Temperature °C		Concentration (%)		Enthalpy (kJ/kg)	
1	Ref [3]	Present	Ref [3]	Present	Ref [3]	Present
2	35	35	55.30	55.211	85.331	84.070
3	35	35	55.30	55.211	85.331	84.070
4	62	61.9	55.30	55.211	140.314	139.451
5	80	80	60.3	60.312	195.808	194.210
6	48.5	48.5	60.3	60.312	135.625	133.712
7	48.5	48.5	60.3	60.312	135.625	133.712
8	80	80	0	0	2650.317	2651.317
9	35	35	0	0	146.772	146.630
10	5	5	0	0	146.772	146.630

Figure 11.11 compares the estimations of the present model at three values of the generator temperature with those obtained by Abdulateef et. al. [3] for the heat removed in the absorber (Q_a), the heat added in the absorber generator (Q_g), the heat added in the

evaporator (Q_e), the heat removed in the condenser (Q_c), and the COP. Unlike the heat transfer in the evaporator (Q_e) and condenser (Q_c) where the fluid is pure water, estimates of both Q_a and Q_g depend on the accuracy of estimating the enthalpy of the LiBr-water solution. The figure shows that Thermax functions give accurate estimations of the variation of all four heat-transfer rates as well as the COP.

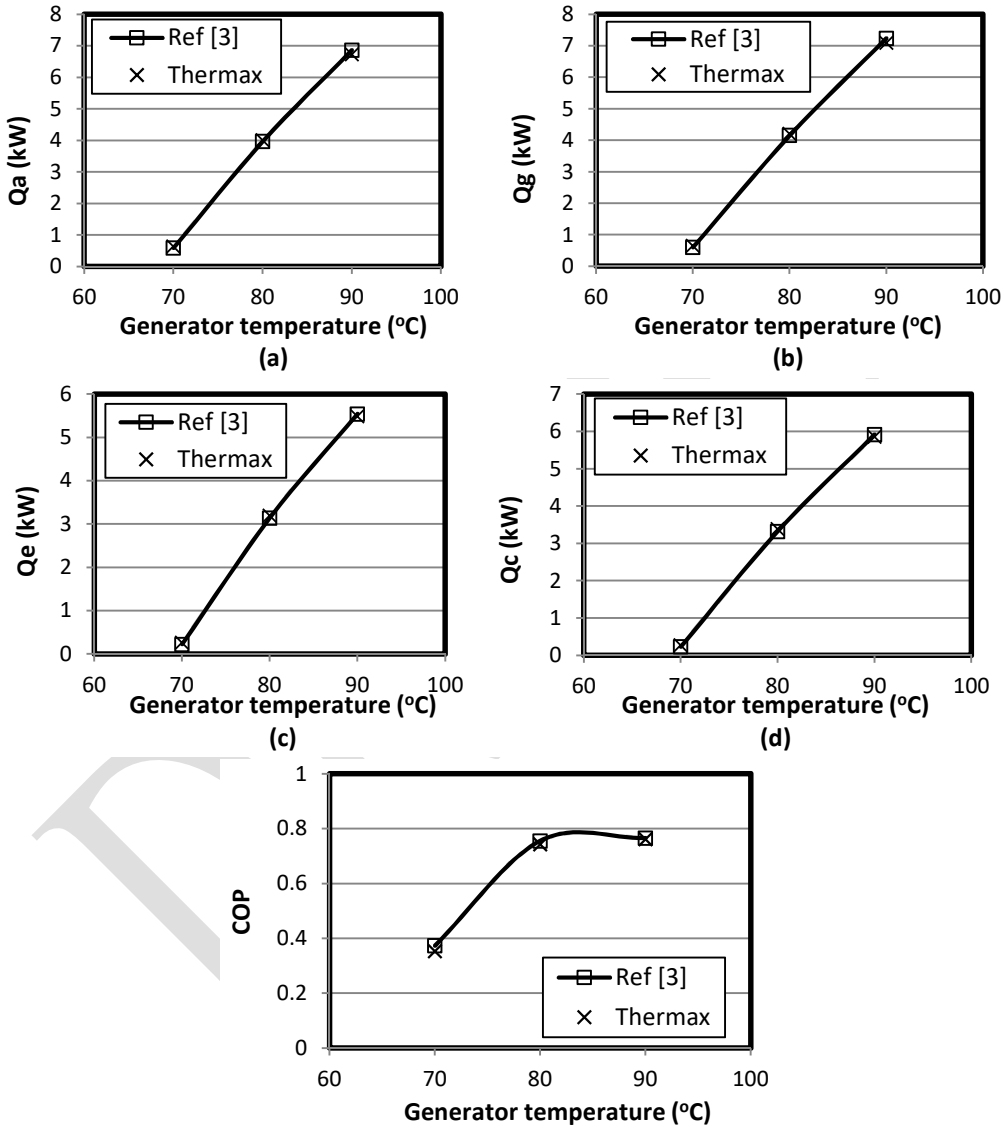

Figure 11.11. Variations of (a) evaporator heat, (b) condenser heat, (c) absorber heat (d) generator heat and (e) COP with generator temperature

Figure 11.11.e shows that the system's COP achieves a constant value of nearly 0.8 between 80°C and 90°C, but drops significantly at the generator temperature of 70°C.

This figure proves what has been mentioned earlier that the COP of a single-effect lithium-bromide-water system becomes essentially independent of the heat input temperature above a certain value and remains constant [10]. Single effect systems usually operate with hot water temperature ranging from 80°C with unpressurised hot water to 120°C with pressurised hot water [4]. When superheated steam at a higher temperature is available, a double-effect cycle can be used. As shown below, by incorporating an additional generator the double-effect system improves the COP to almost twice its value for the single-effect system.

11.5. Analysis of the double-effect parallel-flow system

Figure 11.12 shows the schematic diagram of a double-effect VAR system that uses a high-temperature heat source to drive two generators. The first, high-pressure generator separates the refrigerant from the absorbent and the vapour produced here moves to the condenser where it is condensed into a liquid. The diluted absorbent then flows to a second, low-pressure generator where the heat from the condenser is used to further separate the refrigerant from the solution. The resulting vapour is taken to a second low-pressure condenser. The liquid refrigerant from the two condensers then flows to the evaporator where it evaporates, creating the cooling effect. This system increases the cooling capacity and improves the overall operating efficiency.

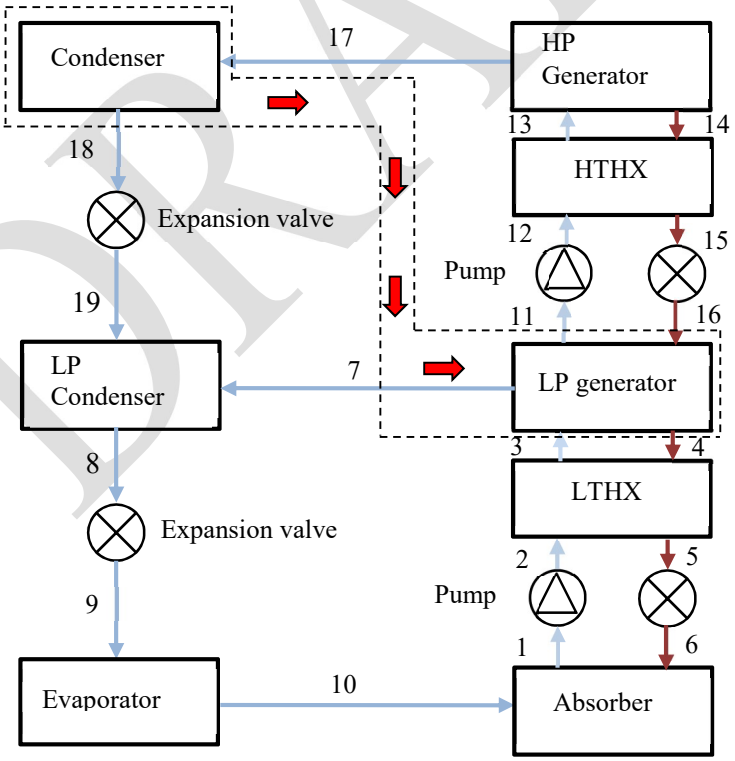

Figure 11.12. Schematic of double-effect VAR system in parallel flow scheme

DRAFT

Two main circulation methods for the strong and weak solutions can be defined for double-effect VAR cycles: the parallel flow mode and the series flow mode. The system shown in Figure 11.12 is a parallel-flow double-effect system. In the series-flow system, the outlet dilute soluble from the absorber is pumped into the low-temperature heat-exchanger, and then let into the high-temperature heat-exchanger and afterwards directly into the high-temperature generator. Therefore, this system needs a single pump to drive the weak solution to the high-pressure generator. Like the parallel-flow cycle, there are three pressure levels in this cycle and the water vapour taken from the weak solution in each generator enters a distinct condenser [13]. The double-effect VAR system considered in the following analysis is a parallel-flow system that uses a water-lithium bromide solution with the particulars shown on Table 11.4 as given by ASHRAE [2].

Table 11.4. Inputs for the model of the double-effect system

Input	Value
Capacity (Q_e)	1760 kW
Evaporator temperature (T_{10})	5°C
Desorber solution exit temperature (T_{14})	170.7°C
Condenser/absorber low temperature ($T_1 = T_8$)	42.4°C
Temperature difference between the high-temperature condenser T_{18} and low-temperature generator T_4	5ºC
Solution heat exchanger effectiveness (ε)	0.6

11.5.1. The analytical model

Following ASHRAE, mass and energy balances of the system are calculated with the following assumptions:

- The refrigerant solution is saturated after it passes through the absorber and the generator, i.e., state points at 1, 4, 11, and 14.
- State points at 8 and 18 are saturated liquid water.
- Upper loop solution flow rate is selected such that upper condenser heat exactly matches lower generator heat requirement
- Vapour leaving both generators, i.e. T_7 and T_{17}, is at equilibrium temperatures of entering solution streams. State points at 7 and 17 are superheated water vapour.

Since the temperatures at the evaporator and low-temperature condenser are known, the low and intermediate pressure levels can be determined at these temperatures from the properties of saturated water. However, the high pressure level at the HTC and HTG depends on the temperature at state point 4 or 18 which are not specified. Since the difference between T_{18} and T_4 is specified as 5ºC, determining one of the temperatures will fix the other. The following Excel-based model assumes initial values for T_4 which is then adjusted by using Excel's Solver to satisfy all the mass and energy balances in the cycle. This approach is similar to that adopted by Yılmaz et al. [14].

DRAFT

The solution concentrations at points 1 and 4 can be determined from the known values of the temperatures and pressures using Thermax function **LibX_PrT** and the enthalpies h_1 and h_4 can then be determined by using the function **LiBh_TX**. The concentrations of the solution at state points 11 and 14 are takes as equal to those at 1 and 4, respectively. Accordingly:

$$X_{11} = X_{12} = X_{13} = X_1 \tag{11.29}$$

$$X_{13} = X_{14} = X_{15} = X_4 \tag{11.30}$$

The temperatures of the weak solution after the two heat-exchangers at state points 3 and 13 are determined as follows:

$$T_3 = T_2 + \varepsilon\left(T_4 - T_2\right) \tag{11.31}$$

$$T_{13} = T_{12} + \varepsilon\left(T_{14} - T_{12}\right) \tag{11.32}$$

The enthalpies at state points 3 and 13 are determined by using the function **LiBh_TX** from which the enthalpies at state points 5 and 15 are determined from energy balances:

$$h_5 = h_4 - \left(\dot{m}_1 / \dot{m}_5\right)\left(h_3 - h_2\right) \tag{11.33}$$

$$h_{15} = h_{14} - \left(\dot{m}_{11} / \dot{m}_{15}\right)\left(h_{13} - h_{12}\right) \tag{11.34}$$

The temperatures T_5 and T_{15} are then determined by using the function **LiBT_hX**.

Since the flow restrictors are adiabatic, the enthalpies of the strong solution h_6 and h_{16} are given by:

$$h_6 = h_5 \tag{11.35}$$

$$h_{16} = h_{15} \tag{11.36}$$

Similarly, enthalpies of the pure refrigerant h_9 and h_{19} given by:

$$h_9 = h_8 \tag{11.37}$$

$$h_{19} = h_{18} \tag{11.38}$$

The temperatures T_6 and T_{16} are then determined from the known values of enthalpy and concentration using the function **LibT_hX**. Neglecting the work in the two pumps, the

DRAFT

temperatures and enthalpy values at state points 2 and 12 after the pumps were taken as equal to their corresponding values at points 1 and 11 before the pumps.

The mass flow rates of the water vapour in and out the evaporator are determined from the specified cooling capacity, Q_e, as follows:

$$\dot{m}_9 = \dot{m}_{10} = Q_e / (h_{10} - h_9) \tag{11.39}$$

The other mass flow rates are determined as follows:

$$\dot{m}_1 = \dot{m}_{10} + \dot{m}_6 \tag{11.40}$$

$$\dot{m}_3 = \dot{m}_2 = \dot{m}_1 \tag{11.41}$$

$$\dot{m}_4 = \dot{m}_3 X_3 / X_4 \tag{11.42}$$

$$\dot{m}_6 = \dot{m}_5 = \dot{m}_4 \tag{11.43}$$

$$\dot{m}_7 = \dot{m}_3 - \dot{m}_4 - \dot{m}_{11} + \dot{m}_{16} \tag{11.44}$$

$$\dot{m}_8 = \dot{m}_9 \tag{11.45}$$

$$\dot{m}_{16} = \dot{m}_{11} X_{11} / X_{16} \tag{11.46}$$

$$\dot{m}_{14} = \dot{m}_{15} = \dot{m}_{16} \tag{11.47}$$

$$\dot{m}_{11} = \dot{m}_{16} + \dot{m}_{17} \tag{11.48}$$

Heat and work transfer rates;

$$Q_{\text{evap}} = \dot{m}_9 (h_{10} - h_9) \tag{11.49}$$

$$Q_{\text{abs}} = \dot{m}_{10} h_{10} + \dot{m}_6 h_6 - m_1 h_1 \tag{11.50}$$

$$Q_{\text{cond}} = \dot{m}_7 h_7 + \dot{m}_{19} h_{19} - \dot{m}_8 h_8 \tag{11.51}$$

$$Q_{lpg} = \dot{m}_7 h_7 + \dot{m}_{11} h_{11} - \dot{m}_{16} h_{16} - \dot{m}_3 h_3 + \dot{m}_4 h_4 \tag{11.52}$$

$$Q_{hpc} = \dot{m}_{17} (h_{17} - h_{18}) \tag{11.53}$$

DRAFT

$$W_{pump1} = \dot{m}_1 v_1 \left(P_{LTG} - P_{evap} \right) \tag{11.54}$$

$$W_{pump2} = \dot{m}_{11} v_{11} \left(P_{HTG} - P_{LTG} \right) \tag{11.55}$$

Energy balance over the HTC and LPG

$$Q_{hpc} = Q_{lpg} \tag{11.56}$$

Overall energy balance:

$$Q_{evap} + Q_{hpg} + W_{pump} = Q_{cond} + Q_{abs} \tag{11.57}$$

This analysis is more challenging than the previous analyses, not only because of the larger number of mass, energy, and concentration equations it involves, but also because all the mass flow rates have to be determined by the analysis. As shown below, the inter-dependence between mass and energy flow rates and solution concentration makes it necessary to adopt the iterative solution procedure.

11.6.2. The Excel model

Figure 11.13 shows the Excel sheet developed for the analysis and Figure 11.14 reveals the formulae used in it with Thermax functions. The system's data given in Table 11.4 are stored on the top left side of the sheet. An initial value for T_4 of 100ºC is assumed. The sheet then determines the various pressures in the system's components. At the initial value of T_4, Figure 11.13 shows that the rates of heat transfer in the HTC and LTG are not equal and, therefore, Equation (11.56) is not satisfied. The figure also shows that the calculations of the mass flow rates $\dot{m}_1$, $\dot{m}_3$, $\dot{m}_4$ and $\dot{m}_6$ leads to circular calculations.

Diff =ABS(Q_ch-Q_gl)

	A	B	C	D	E	F	G	H	I	J	K	L	M	N	O	P	Q	R
1	Input data																	
2	Q_E	1760	kW	T_1	42.4		x_1	59.060		m_1	8.246		h_1	115.523		Energy balance		
3	T_E	5	oC	T_2	42.4		x_2	59.060		m_2	8.246		h_2	115.523		Q_ch	904.8387	
4	T_HTG	170.7	oC	T_3	76.96		x_3	59.060		m_3	8.246		h_3	183.137		Q_gl	1183.143	
5	T_A	42.4	oC				x_4	65.009		m_4	7.491		h_4	253.282				
6				T_5	58.431		x_5	65.009		m_5	7.491		h_5	178.857		Q_a	2281.264	
7	ε	0.6		T_6	54.525		x_6	65.009		m_6	7.491		h_6	178.857		Q_c	1020.181	
8				T_7	85.788		x_7	0		m_7	0.370		h_7	2662.036		Q_gh	1263.141	
9	T_4	100	oC	T_8	42.4		x_8	0		m_8	0.755		h_8	177.562				
10				T_9	5		x_9	0		m_9	0.755		h_9	177.562		Q_shx1	557.531	
11	P_E	0.870	kPa	T_10	5		x_10	0		m_10	0.755		h_10	2510.060		Q_shx2	419.646	
12	P_A	0.870	kPa															
13	P_cl	8.441	kPa	T_11	85.788		x_11	59.060		m_11	4.203		h_11	200.422		w_p1	0.037	
14	P_gl	8.441	kPa	T_12	85.788		x_12	59.060		m_12	4.203		h_12	200.422		w_p2	0.284	
15				T_13	136.735		x_13	59.060		m_13	4.203		h_13	300.268				
16	P_ch	120.900	kPa	T_14	170.7		x_14	65.009		m_14	3.818		h_14	380.005		COP	1.393	
17	P_gh	120.900	kPa	T_15	109.389		x_15	65.009		m_15	3.818		h_15	270.101				
18				T_16	100.000		x_16	65.0091		m_16	3.818		h_16	270.101		Diff	278.3042	
19	v_1	0.00059		T_17	158.433		x_17	0		m_17	0.385		h_17	2792.940				
20	v_11	0.000601		T_18	105		x_18	0		m_18	0.385		h_18	440.270				
21				T_19	42.367		x_19	0		m_19	0.385		h_19	440.270				
22																		

Figure 11.13. The sheet developed for analysing the double-effect VAR system

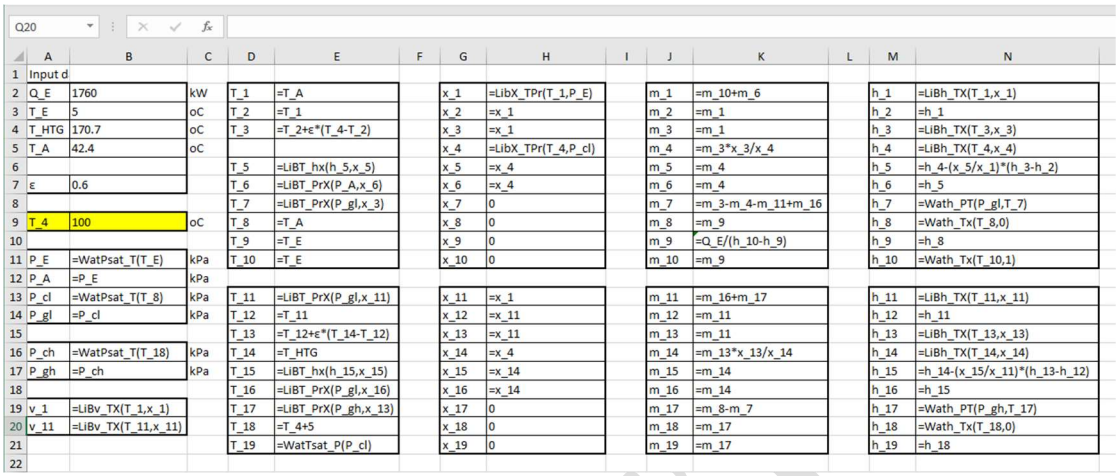

	A	B	C	D	E	F	G	H	I	J	K	L	M	N
1	Input d													
2	Q_E	1760	kW	T_1	=T_A		x_1	=LibX_TPr(T_1,P_E)		m_1	=m_10+m_6		h_1	=LiBh_TX(T_1,x_1)
3	T_E	5	oC	T_2	=T_1		x_2	=x_1		m_2	=m_1		h_2	=h_1
4	T_HTG	170.7	oC	T_3	=T_2+ε*(T_4-T_2)		x_3	=x_1		m_3	=m_1		h_3	=LiBh_TX(T_3,x_3)
5	T_A	42.4	oC				x_4	=LibX_TPr(T_4,P_cl)		m_4	=m_3*x_3/x_4		h_4	=LiBh_TX(T_4,x_4)
6				T_5	=LiBT_hx(h_5,x_5)		x_5	=x_4		m_5	=m_4		h_5	=h_4-(x_5/x_1)*(h_3-h_2)
7	ε	0.6		T_6	=LiBT_PrX(P_A,x_6)		x_6	=x_4		m_6	=m_4		h_6	=h_5
8				T_7	=LiBT_PrX(P_gl,x_3)		x_7	0		m_7	=m_3-m_4-m_11+m_16		h_7	=Wath_PT(P_gl,T_7)
9	T_4	100	oC	T_8	=T_A		x_8	0		m_8	=m_9		h_8	=Wath_Tx(T_8,0)
10				T_9	=T_E		x_9	0		m_9	=Q_E/(h_10-h_9)		h_9	=h_8
11	P_E	=WatPsat_T(T_E)	kPa	T_10	=T_E		x_10	0		m_10	=m_9		h_10	=Wath_Tx(T_10,1)
12	P_A	=P_E	kPa											
13	P_cl	=WatPsat_T(T_8)	kPa	T_11	=LiBT_PrX(P_gl,x_11)		x_11	=x_1		m_11	=m_16+m_17		h_11	=LiBh_TX(T_11,x_11)
14	P_gl	=P_cl	kPa	T_12	=T_11		x_12	=x_11		m_12	=m_11		h_12	=h_11
15				T_13	=T_12+ε*(T_14-T_12)		x_13	=x_11		m_13	=m_11		h_13	=LiBh_TX(T_13,x_13)
16	P_ch	=WatPsat_T(T_18)	kPa	T_14	=T_HTG		x_14	=x_4		m_14	=m_13*x_13/x_14		h_14	=LiBh_TX(T_14,x_14)
17	P_gh	=P_ch	kPa	T_15	=LiBT_hx(h_15,x_15)		x_15	=x_14		m_15	=m_14		h_15	=h_14-(x_15/x_11)*(h_13-h_12)
18				T_16	=LiBT_PrX(P_gl,x_16)		x_16	=x_14		m_16	=m_14		h_16	=h_15
19	v_1	=LiBv_TX(T_1,x_1)		T_17	=LiBT_PrX(P_gh,x_13)		x_17	0		m_17	=m_8-m_7		h_17	=Wath_PT(P_gh,T_17)
20	v_11	=LiBv_TX(T_11,x_11)		T_18	=T_4+5		x_18	0		m_18	=m_17		h_18	=Wath_Tx(T_18,0)
21				T_19	=WatTsat_P(P_cl)		x_19	0		m_19	=m_17		h_19	=h_18
22														

Figure 11.14. The formulae used for analysing the parallel-flow double effect water-lithium bromide VAR system

Circular calculations indicate that the number of equations are less than the number of unknowns. While Solver determines the value of T_4 that satisfies Equation (11.56), the iterative solution option of Excel determines the required mass-flow rates. Figure 11.15 shows Solver's set-up for determining the temperature T_4 and Figure 11.16 shows its solution by using the GRG Nonlinear method with automatic-scaling.

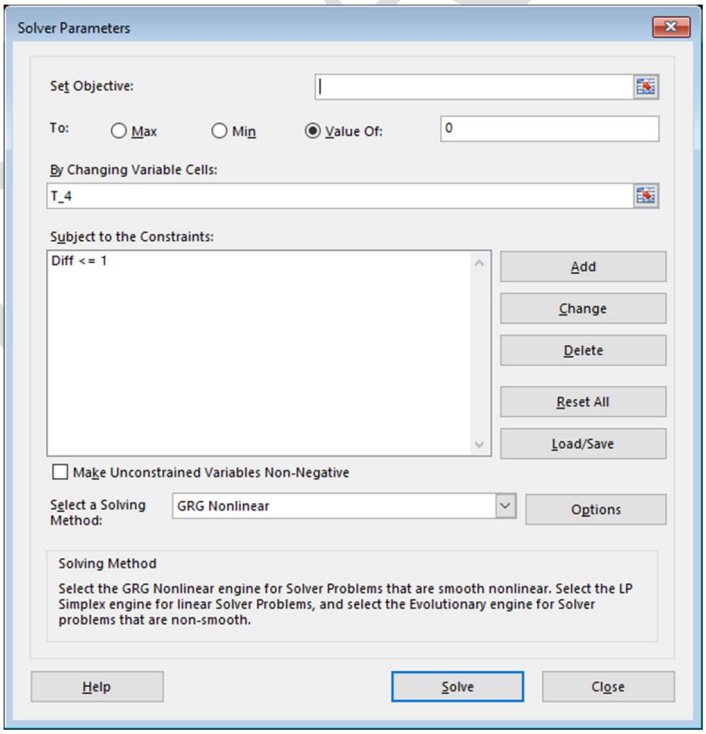

Figure 11.15. Solver's set-up for analysing the double-effect VAR system

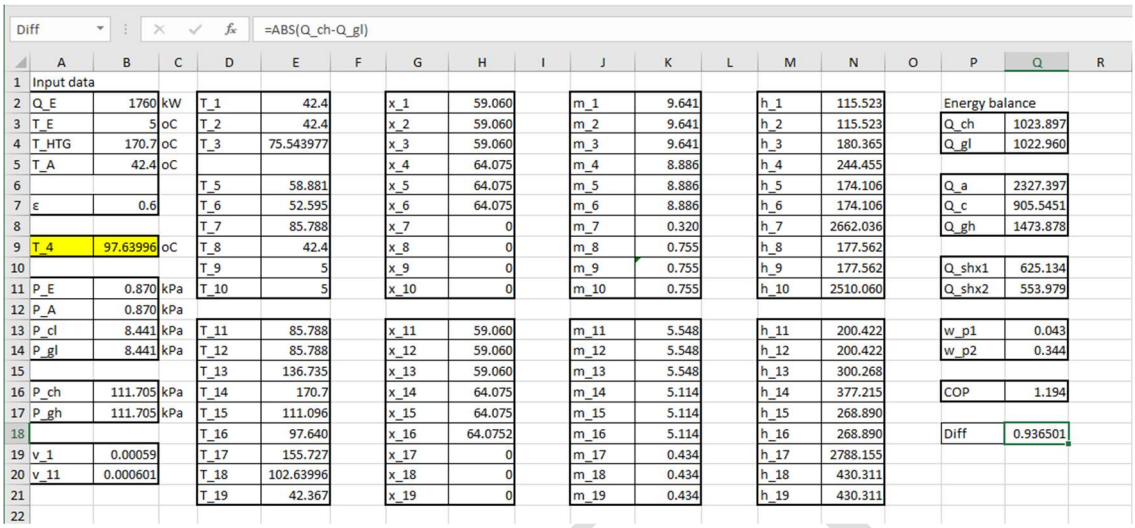

Diff | =ABS(Q_ch-Q_gl)

	A	B	C	D	E	G	H	J	K	M	N	P	Q
1	Input data												
2	Q_E	1760	kW	T_1	42.4	x_1	59.060	m_1	9.641	h_1	115.523	Energy balance	
3	T_E	5	oC	T_2	42.4	x_2	59.060	m_2	9.641	h_2	115.523	Q_ch	1023.897
4	T_HTG	170.7	oC	T_3	75.543977	x_3	59.060	m_3	9.641	h_3	180.365	Q_gl	1022.960
5	T_A	42.4	oC			x_4	64.075	m_4	8.886	h_4	244.455		
6				T_5	58.881	x_5	64.075	m_5	8.886	h_5	174.106	Q_a	2327.397
7	ε	0.6		T_6	52.595	x_6	64.075	m_6	8.886	h_6	174.106	Q_c	905.5451
8				T_7	85.788	x_7	0	m_7	0.320	h_7	2662.036	Q_gh	1473.878
9	T_4	97.63996	oC	T_8	42.4	x_8	0	m_8	0.755	h_8	177.562		
10				T_9	5	x_9	0	m_9	0.755	h_9	177.562	Q_shx1	625.134
11	P_E	0.870	kPa	T_10	5	x_10	0	m_10	0.755	h_10	2510.060	Q_shx2	553.979
12	P_A	0.870	kPa										
13	P_cl	8.441	kPa	T_11	85.788	x_11	59.060	m_11	5.548	h_11	200.422	w_p1	0.043
14	P_gl	8.441	kPa	T_12	85.788	x_12	59.060	m_12	5.548	h_12	200.422	w_p2	0.344
15				T_13	136.735	x_13	59.060	m_13	5.548	h_13	300.268		
16	P_ch	111.705	kPa	T_14	170.7	x_14	64.075	m_14	5.114	h_14	377.215	COP	1.194
17	P_gh	111.705	kPa	T_15	111.096	x_15	64.075	m_15	5.114	h_15	268.890		
18				T_16	97.640	x_16	64.0752	m_16	5.114	h_16	268.890	Diff	0.936501
19	v_1	0.00059		T_17	155.727	x_17	0	m_17	0.434	h_17	2788.155		
20	v_11	0.000601		T_18	102.63996	x_18	0	m_18	0.434	h_18	430.311		
21				T_19	42.367	x_19	0	m_19	0.434	h_19	430.311		
22													

Figure 11.16. Solver's solution of the double-effect VAR system

Figure 11.16 shows that the value of T_4 determined by Solver is 97.64ºC. Table 11.5 shows the values obtained by the Excel-Thermax model for the mass flow rate ($\dot{m}$), refrigerant concentration (X), solution temperature (T), and solution enthalpy (h) and Figure 11.17 shows the percentage deviation of these results from those given by [2].

Table 11.5. Results of the double-effect VAR cycle analysis

#	$\dot{m}$	X	T	h
1	9.641	59.060	42.4	115.523
2	9.641	59.060	42.4	115.523
3	9.641	59.060	75.54397	180.365
4	8.886	64.075	97.6399	244.455
5	8.886	64.075	58.881	174.106
6	8.886	64.075	52.595	174.106
7	0.320	0	85.788	2662.036
8	0.755	0	42.4	177.562
9	0.755	0	5	177.562
10	0.755	0	5	2510.060
11	5.548	59.060	85.788	200.422
12	5.548	59.060	85.788	200.422
13	5.548	59.060	136.735	300.268
14	5.114	64.075	170.7	377.215
15	5.114	64.075	111.096	268.890
16	5.114	64.075	97.640	268.890
17	0.434	0	155.727	2788.155
18	0.434	0	102.6399	430.311
19	0.434	0	42.367	430.311

DRAFT

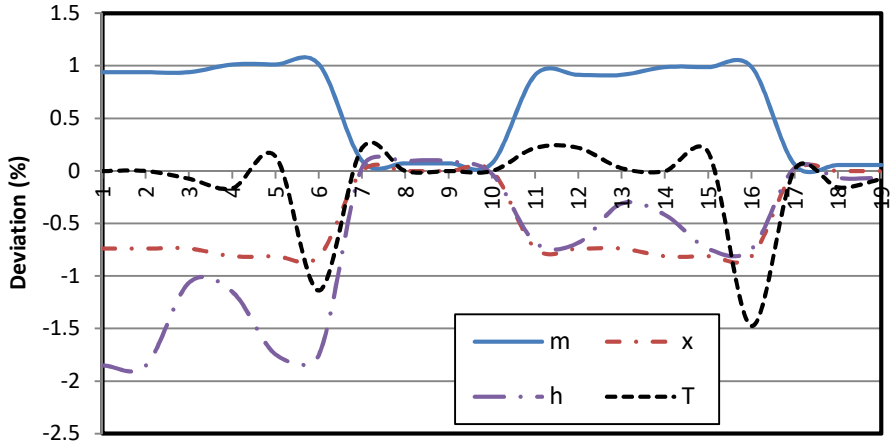

Figure 11.17. Percentage deviations from ASHRAE [2] data

Figure 11.17 shows that most of the values deviated by less than 1% from their corresponding values given by ASHRAE [2]. Table 11.6 compares the different pressures and heat-transfer rates in the system's components as obtained by the present model with those given by ASHRAE [2]. The table, which also shows the pumps work and cycle COP, shows excellent agreements with the reference data. The calculated COP, in particular, is in close agreement with that given by ASHRAE [2].

Table 11.6. Comparison of the present estimations with those of Ref. [2]

	Ref. [2]	Present	% error
Evaporator pressure	0.88	0.870	1.14
Low-temperature generator pressure	8.36	8.441	-0.97
High-temperature generator pressure	111.8	111.705	0.08
Heat-transfer in absorber	2328	2327.397	0.03
Heat-transfer in low-temperature generator	1023	1022.960	0.00
Heat-transfer in low-temperature condenser	905	905.545	-0.06
Heat-transfer in high-temperature generator	1472	1473.879	-0.13
Heat-transfer in heat-exchanger 1	617	625.134	-1.32
Heat-transfer in heat-exchanger 2	546	553.980	-1.46
Work supplied to pump 1	0.043	0.043	-0.66
Work supplied to pump 2	0.346	0.344	0.51
COP	1.195	1.194	0.10

Figure 11.16 shows that the COP of the double-effect system is approximately 1.2. Compared to the COP of the single-effect system considered in Example 11.4, which operates at the same evaporator temperature, the COP of the double-effect system is almost double. A number of studies also show that the COP of the parallel-flow double-effect system is higher than that the series-flow double-effect system [10,12-15]. However, the series-flow system is easier to control than the parallel-flow one [9].

11.6. Analysis of the single-effect VAR cycle using water-ammonia solution

Thermax group of functions for the water-ammonia solution (NH3) also provides thirteen functions that can be used for energy and exergy analyses of various types of VAR systems. The following example demonstrates their use by analysing the single-effect system with a heat exchanger considered in Example 11.4 using the data provided by Sun [4]. The analytical model for the system is described in Section 11.4.1.

Example 11.5. Analysis of the single-effect system with a water-ammonia solution

Analyse the performance of the single-effect VAR system shown on Figure 11.6 with water-ammonia as the working fluid using the following data;

T_g = 100°C,
T_c = 30°C,
T_a=25°C,
T_e = -5°C,
The refrigerant mass flow rate is 1 kg/min,
The heat-exchanger effectiveness is 80%.

The Excel sheet

Figure 11.18 shows the Excel sheet prepared for this example by applying the analytical model described in Section 11.4.1, but using Thermax functions for the ammonia-water solution. Figure 11.19 reveals the formulae used in the sheet. Note that the concentration X here refers to that of ammonia in water. Therefore, the value of X at state 7, which is pure ammonia, is 100%. Table 11.7 compares the cycle parameters as obtained by the model and those given by Sun [4]. The figures of the table show good agreement between the estimations of the two analyses. The cycle's COP of 0.6 is typical for ammonia-water systems [11].

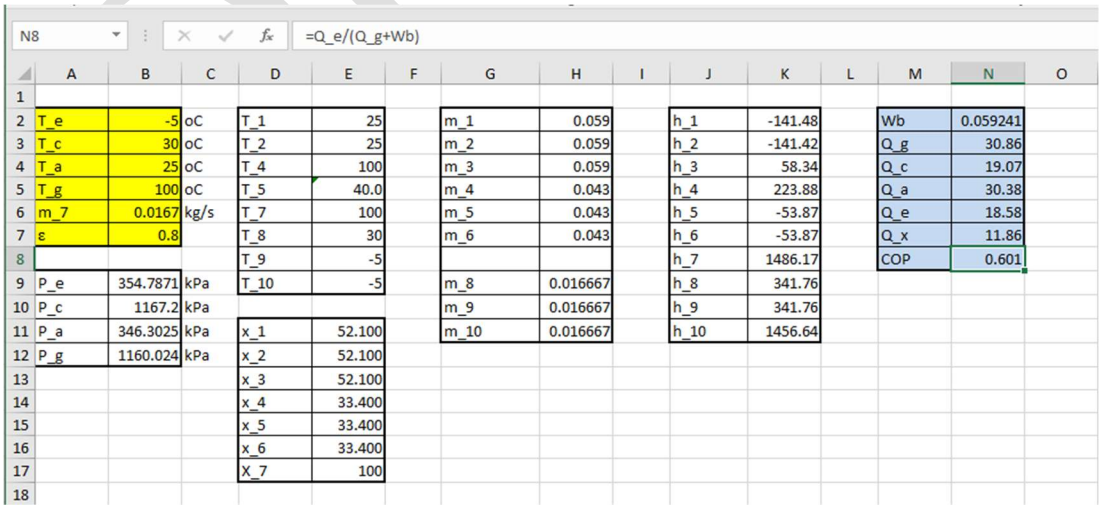

Figure 11.18. Excel sheet developed for the ammonia-water VAR system

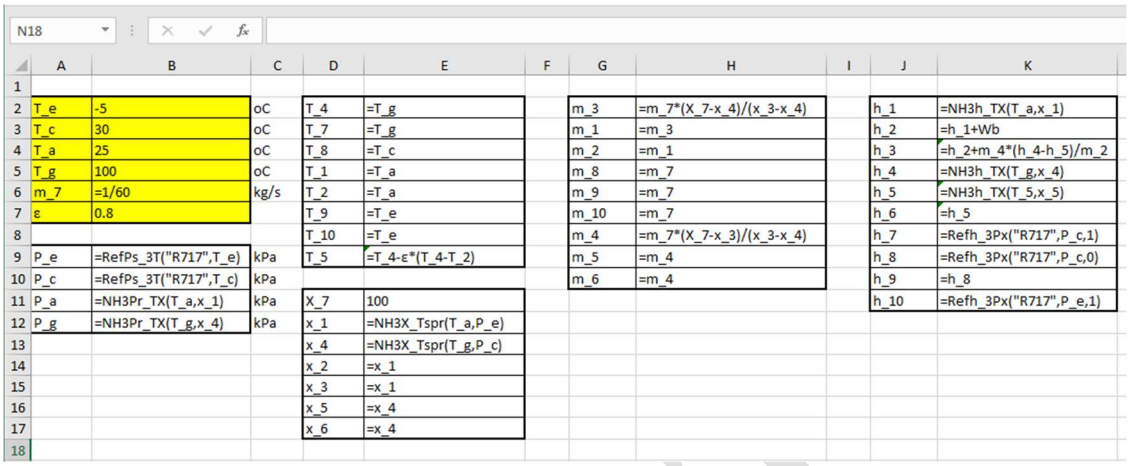

	A	B	C	D	E	F	G	H	I	J	K
1											
2	T_e	-5	oC	T_4	=T_g		m_3	=m_7*(X_7-x_4)/(x_3-x_4)		h_1	=NH3h_TX(T_a,x_1)
3	T_c	30	oC	T_7	=T_g		m_1	=m_3		h_2	=h_1+Wb
4	T_a	25	oC	T_8	=T_c		m_2	=m_1		h_3	=h_2+m_4*(h_4-h_5)/m_2
5	T_g	100	oC	T_1	=T_a		m_8	=m_7		h_4	=NH3h_TX(T_g,x_4)
6	m_7	=1/60	kg/s	T_2	=T_a		m_9	=m_7		h_5	=NH3h_TX(T_5,x_5)
7	ε	0.8		T_9	=T_e		m_10	=m_7		h_6	=h_5
8				T_10	=T_e		m_4	=m_7*(X_7-x_3)/(x_3-x_4)		h_7	=Refh_3Px("R717",P_c,1)
9	P_e	=RefPs_3T("R717",T_e)	kPa	T_5	=T_4-ε*(T_4-T_2)		m_5	=m_4		h_8	=Refh_3Px("R717",P_c,0)
10	P_c	=RefPs_3T("R717",T_c)	kPa				m_6	=m_4		h_9	=h_8
11	P_a	=NH3Pr_TX(T_a,x_1)	kPa	X_7	100					h_10	=Refh_3Px("R717",P_e,1)
12	P_g	=NH3Pr_TX(T_g,x_4)	kPa	x_1	=NH3X_Tspr(T_a,P_e)						
13				x_4	=NH3X_Tspr(T_g,P_c)						
14				x_2	=x_1						
15				x_3	=x_1						
16				x_5	=x_4						
17				x_6	=x_4						
18											

Figure 11.19. The formulae in the Excel sheet of Figure 11.18 for the VAR system

Table 11.7. Verification of Thermax functions for ammonia-water VAR system

	Sun [4]	Present	Error (%)
Q_g (kW)	30.1314	30.86	2.42
Q_c (kW)	18.4611	19.07	3.30
Q_e (kW)	18.5974	18.58	-0.09
Q_a (kW)	30.3269	30.38	0.18
W_p (kW)	0.0592	0.059	-0.34
Q_{ex} (kW)	11.8382	11.86	0.18
COP	0.6160	0.601	-2.44

The cycle's COP is lower than those of the two single–effect systems considered in Example 11.3 and Example 11.4 using Li-Br-water solution, which are 0.688 and 0.761, respectively. One reason for this is the lower evaporator temperature. To evaluate the system's performance by excluding the effect of the evaporator temperature in the water-ammonia system, the sheet was modified to suit the same operating condition of that of the system in Example 11.4. Figure 11.20 that shows the modified Excel sheet indicates that the COP of the water-ammonia system dropped slightly to 0.597. As shown in Table 11.8 that compares the two pressure levels in the system, the operating pressures with the ammonia-water solution are much higher than those with the Li-Br-water solution.

11.7. Closure

The chapter illustrates the use of Thermax property functions for first-law analyses of vapour-absorption refrigeration cycles that include the basic cycle, the single-effect cycle with a single heat-exchanger, and the parallel-flow double effect cycle. For the single-effect cycle, the results are obtained with the two binary solutions; water-lithium-bromide and ammonia-water. Comparisons of the results obtained with relevant published data for the cases considered confirm the adequacy of the property functions. Appendix F extends the treatment of this chapter by analysing a series-flow double-effect system

DRAFT

using a water-lithium-bromide solution with the data given by Kaynakli et al. [16] and by presenting exergy as well as energy analyses of the system.

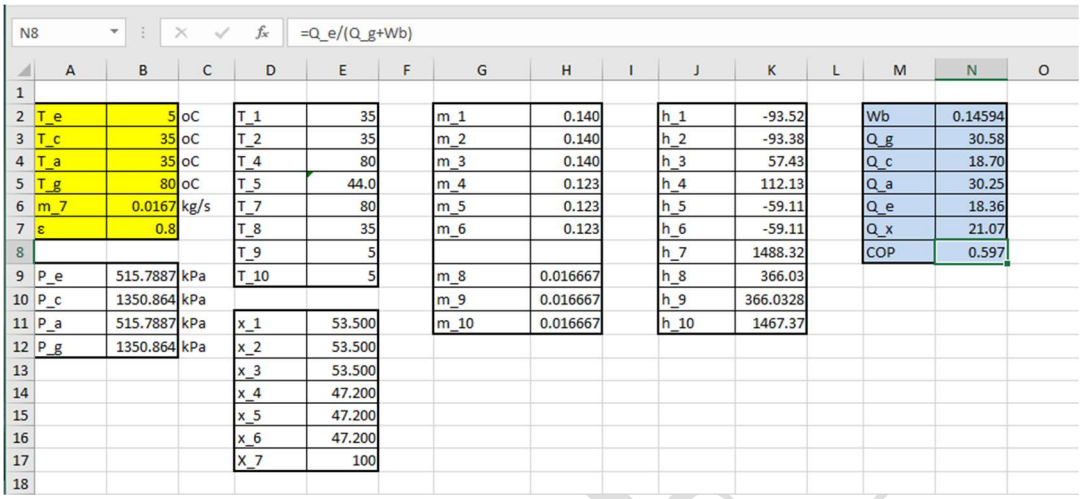

N8 =Q_e/(Q_g+Wb)

	A	B	C	D	E	F	G	H	I	J	K	L	M	N	O
1															
2	T_e	5	oC	T_1	35		m_1	0.140		h_1	-93.52		Wb	0.14594	
3	T_c	35	oC	T_2	35		m_2	0.140		h_2	-93.38		Q_g	30.58	
4	T_a	35	oC	T_4	80		m_3	0.140		h_3	57.43		Q_c	18.70	
5	T_g	80	oC	T_5	44.0		m_4	0.123		h_4	112.13		Q_a	30.25	
6	m_7	0.0167	kg/s	T_7	80		m_5	0.123		h_5	-59.11		Q_e	18.36	
7	ε	0.8		T_8	35		m_6	0.123		h_6	-59.11		Q_x	21.07	
8				T_9	5					h_7	1488.32		COP	0.597	
9	P_e	515.7887	kPa	T_10	5		m_8	0.016667		h_8	366.03				
10	P_c	1350.864	kPa				m_9	0.016667		h_9	366.0328				
11	P_a	515.7887	kPa	x_1	53.500		m_10	0.016667		h_10	1467.37				
12	P_g	1350.864	kPa	x_2	53.500										
13				x_3	53.500										
14				x_4	47.200										
15				x_5	47.200										
16				x_6	47.200										
17				X_7	100										
18															

Figure 11.20. Performance of the single-effect VAR system using the water-ammonia solution under the same operating conditions of Example 11.4

Table 11.8. Comparison of the operating pressures with the two solutions

	LiBr-water	Ammonia-water
Evaporator/absorber pressure, kPa	0.87	515.789
Condenser/generator pressure, kPa	5.63	1350.864

Because of their cruicial role for utilising low-grade and renewable energy sources, a lot of research has been done on the development of VAR systems. Therefore, VAR systems have more design configurations than VCR systems. In addition to the standard single-effect systems and the parallel and series flow configurations, there are designs with a reverse parallel-flow and a parallel-flow with a single pump [10,13,14]. Twelve possible flow configurations have been identified for tripple-effect systems [2]. Even the simple single-effect system has been designed with multi-lifts and with ejectors so as to improve its COP [10,15]. The selection of a suitable VAR system should consider the cost-energy tradeoff between the different refrigeration systems. The single-effect systems are recommended when a simple structure and low cost are pursued, the single-effect double-lift systems are recommended for the utilisation of low temperature heat sources, while the multi-effect systems are recommended for high temperature heat sources [12].

References

[1] W.F. Stoecker and J.W. Jones, *Refrigeration And Air Conditioning*, 2nd edition, McGraw Hill Inc. 1982.

[2] American Society of Heating, Refrigeration and Air-Conditioning Engineers, *Handbook of fundamentals*, Atlanta: ASHRAE 2017

DRAFT

[3] J.M. Abdulateef, M.A. Alghoul, R. Sirwan, A. Zahrim, K. Sopian, Second law thermodynamic analysis of a solar single-stage absorption refrigeration system, *Models and Methods in Applied Sciences,* 2012 pp. 163 – 168.

[4] D-W Sun. Comparison of the performances of NH_3-H_2O, NH_3-$LiNO_3$ and NH_3-NaSCN absorption refrigeration systems. *Energy Convers. Mgmt*, Vol. 39, No. 5/6, 1998, pp. 357-368

[5] S. H. Al-Tahaineh, M. Frihat, M. Al-Rashdan, Exergy Analysis of a Single-Effect Water-Lithium Bromide Absorption Chiller Powered by Waste Energy Source for Different Cooling Capacities, *Energy and Power* 2013, 3(6): 106-118

[6] N. Kurtulmuş, M. Bilgili, B. Şahin, Energy and exergy analysis of a vapor absorption refrigeration system in an intercity bus application, *Journal of Thermal Engineering*, Yildiz Technical University Press, Istanbul, Turkey, Vol. 5, No. 4, pp. 355-371, July, 2019

[7] Md. Meraj, M. Emran Khan, Rashid Imam, Thermodynamic Analysis of Single Effect Vapor Absorption Refrigeration Cycle, *International Journal of Science and Research* (IJSR), ISSN (Online): 2319-7064

[8] N. Sitotaw, Energy and Exergy Analysis of Single Effect Water-LiBr Vapour Absorption Refrigeration System, *International Journal of Advanced Science Computing and Engineering*, Vol. 4, No. 3, December 2022, pp. 175-187

[9] A. Bhatia. Online course. https://www.cedengineering.com/userfiles/M04-025%20%20Overview%20of%20Vapor%20Absorption%20Cooling%20System%20-%20US.pdf

[10] R. Nikbakhti, X. Wang, A. Hussein, and A. Iranmanesh, Absorption cooling systems – Review of various techniques for energy performance enhancement, *Alex. Eng. J.*, vol. 59, pp. 707–738. 2020.

[11] M. Harisha, A.N.R. Reddy, Design of Solar Based Vapour Absorption System, ICEMS-2014

[12] X. Wang and H. T. Chua, Absorption Cooling: A Review of Lithium Bromide-Water Chiller Technologies, Recent Patents on Mechanical Engineering 2009, 2, 193-213 193

[13] F. M. Kashkooli, M. Rezaeian, M. Sefidgar, M. Soltani, M. Mafi, Performance Evaluation of Series and Parallel Two-Stage Absorption Chillers Driven by Solar Energy: Energetic Viewpoint, Gas Processing Journal, Vol. 7, No. 2, 2019

[14] I. H. Yılmaz, K. Saka, Ö. Kaynaklı, Ö. Kaska, Performance Assessment and Solution Procedure for Series Flow Double-Effect Absorption Refrigeration Systems Under Critical Operating Constraints, Arabian Journal for Science and Engineering, March 2019, https://doi.org/10.1007/s13369-019-03805-x

[15] L. Jiang, Z. Gu, X. Feng, Y. Li, Thermo-economical analysis between new absorption–ejector hybrid refrigeration system and small double-effect absorption system, Applied Thermal Engineering 22 (2002) 1027–1036

[16] O. Kaynakli, K. Saka, F. Kaynakli, Energy and exergy analysis of a double effect absorption refrigeration system based on different heat sources, Energy Conversion and Management 106 (2015) 21–30

DRAFT

[17] O. Kaynakli and R. Yamankaradeniz, Thermodynamic analysis of absorption refrigeration system based on entropy generation, Current Science, Vol. 92, No. 4, 25 February 2007

Exercises

1. The basic VAR system shown on Figure 11.1 is modified by the insertion of a heat exchanger between the weak and the strong solutions such that the weak solution enters the generator at a temperature of 55°C. The mass rate of the flow delivered by the pump is 0.6 kg/s. Using Thermax function for H_2O-LiBr solution, determine the rates of energy transfer at each of the components and the COP of this cycle for the same operating temperatures shown on Figure 11.1. This exercise is based on Example 17-4 in Stoecker and Jones [1]. Ans. Q_c = 371.2 kW, Q_e = 348.2 kW, Q_{hx}=28.8 kW, Q_g = 444.5 kW, Q_a=421.3 kW, COP=0.783.
2. Kurtulmuş et al. [6] performed an energy and exergy analysis of the single-effect VAR system shown on Figure 11.6 using the following input parameters:

   T_g = 87.8°C, T_{ev} = 7.2°C, T_{con} = T_{abs} = 37.8°C,
   The effectiveness of solution heat exchanger, ε = 0.7,
   The refrigerant mass flow rate, $\dot{m}_{10}$ = 1 kg/s.

   By suitably modifying the data part of the Excel sheet developed for Example 11.4, analyse the system with the input data of Ref. [6] and compare the two results.
3. The system shown on Figure 11.P3 adds a second heat-exchanger to the single-effect system shown on Figure 11.6. Extend the Excel sheet developed for Example 11.4 to analyse this modified system using a LiBr-water solution with the same input data of Example 11.4 and compare the results with those of the unmodified system.

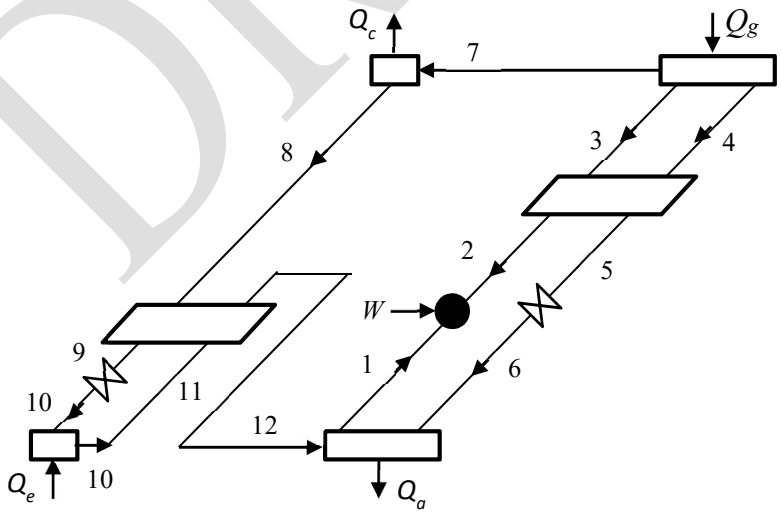

Figure 11.P3. A modified single-effect VAR system

DRAFT

4. Kaynakli and Yamankaradeniz [17] analysed the modified single-effect system shown on Figure 11.P3 for a 10 kW cooling load with the following parameters:

   $T_E = 4°C$, $T_C = 38°C$, $T_A = T_C + 2°C$, $T_G = 90°C$,
   $\varepsilon_{SHE} = \varepsilon_{RHE} = 0.50$,
   $\eta_P = 0.90$.

   Analyse the system using a LiBr-water solution and compare your results with those of Ref. [17] for the same capacity and input parameters.
5. The single-effect VAR system shown on Figure 11.P5 was analysed by ASHRAE [2] using the data shown below the figure.

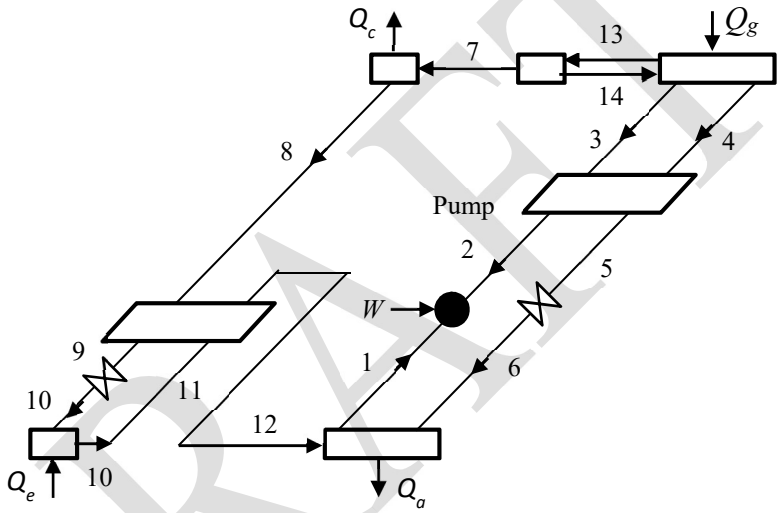

Figure 11.P5. Single-effect ammonia/water absorption cycle

Table 11.P5. Input data for the system in Figure 11.P5

Capacity	1760 kW
High-side pressure	1461 kPa
Low-side pressure	515 kPa
Absorber exit temperature, T_1	40.6 °C
Generator exit temperature, T_4	95 °C
Rectifier vapour exit temperature, T_7	55 °C
Solution heat exchanger effectiveness	0.692
Refrigerant heat exchanger effectiveness	0.629

By using Thermax functions for ammonia-water solution, develop an Excel model to determine the steady-state heat-transfer rates and COP of the system and compare your results with those obtained by ASHRAE [2] with the following assumptions:

- No pressure changes except through flow restrictors and pump

DRAFT

- States at points 1, 4, 8, 11, and 14 are saturated liquid
- States at point 12 and 13 are saturated vapour
- Flow restrictors are adiabatic
- Pump is isentropic
- No jacket heat losses
- No liquid carry-over from evaporator to absorber
- Vapour leaving generator is at equilibrium temperature of entering solution stream

DRAFT